

Contrast Source Inversion-Based Multilayered Object Analysis for Terahertz Wave Imaging

Hayatomomaru Morimoto, Yoshihiro Yamauchi, and Shouhei Kidera^{id}, *Member, IEEE*

Abstract—A complex permittivity profile reconstruction for multilayered objects was presented in this study by incorporating compressed sensing (CS)-based thickness estimation with contrast source inversion (CSI) non-linear inverse scattering (IS) method using a terahertz (THz) frequency band. Several studies investigated permittivity estimation for multiple layers. However, they require a prior knowledge of the thickness of each layer. Moreover, a critical problem in this field is the simultaneous estimation of both the dielectric constant and the thickness of each layer. To address this, a super-resolution thickness estimator using a CS filter and the CSI-based dielectric profile reconstruction scheme was used. This problem was effectively solved by introducing the cost function estimated using the CSI scheme, where the number of layers is given. The finite-difference time-domain (FDTD) numerical test indicated that the proposed method provides an accurate estimation of the thickness and dielectric profile in double-layered objects.

Index Terms—Compressed sensing (CS), contrast source inversion (CSI), multilayer structure analysis, terahertz time-domain spectroscopic (THz-TDS) system.

I. INTRODUCTION

TERAHERTZ (THz)-wave imagers have several advantages, such as a spatial resolution higher than that of millimeter-wave imagers and penetration depth deeper than that obtained by infrared or optical band sensing. Thus, THz-wave imagers are promising candidates for several applications, such as chemical compound analysis [1], subsurface or security screening imaging, [2]–[4] or biological or medical diagnosis [5]. Typically, in a general subsurface imaging scenario, a transmissive response from an object is not possible, and hence, a typical THz imager, such as THz time-domain spectrometer, provides spatial profiles of reflection coefficients using reflection responses [6]. However, these approaches cannot provide a quantitative value of complex permittivity. Quantitatively determining complex permittivity allows the identification of materials and their chemical compound analysis. Several studies proposed a time-of-flight (TOF)-based

permittivity estimation approach [7], assuming a multiple layered object. However, this method requires a prior knowledge of the thickness of each layer, which is not typically available in most scenarios such as security screening or non-destructive inspection. Other studies focused on the thickness estimation for multilayered objects [8], [9]. However, this method requires a prior knowledge of the relative permittivity of each layer.

Inverse scattering (IS) analysis is one of the promising approaches for the simultaneous estimation of thickness and complex permittivity. It has been intensively developed and used in microwave or millimeter-wave imaging applications. In particular, 1-D nonlinear IS has been applied to the 2-D or 3-D multilayered object analysis [10]–[12]. However, in such analyses, mostly a planar incident wave is assumed; this assumption is invalid for the short-range observation model, namely, when the sources and objects are closely located. Then, assuming a typical THz band multilayer analysis, the 2-D or 3-D IS analysis should be considered. However, this is known to be a non-linear and ill-posed inverse problem. A linear-approximation scheme, such as Born approximation, could not offer sufficient accuracy, especially for an object with a high contrast to the background medium. To overcome this problem, numerous IS analysis methods such as distorted Born iterative method (DBIM) [13], contrast source extended Born (CSEB) [14], or contrast source inversion (CSI) [15], [16] are used. Among them, CSI is a highly accurate and low complex method. In CSI, the iterative use of forward solvers, such as finite-difference time-domain (FDTD) method, which require massive computational cost, can be avoided. Nonetheless, the reconstruction profile largely depends on a balance between the number of data samples and that of unknowns or on the selection of the initial estimate of a dielectric profile.

Therefore, this study exploits a prior assumption that each layer of an object has a homogeneous medium to reduce the necessary number of unknowns. Furthermore, to simultaneously provide a thickness of each layer, the method used here incorporates the TOF estimation results provided by a CS filter [17], which has been demonstrated as one of the super-resolution TOF estimators beyond a theoretical depth resolution [9], [18]. Finally, this method introduces a full search for the dielectric constant estimation in each layer using the residual of the cost function obtained by a CSI process, in which the thickness of each layer is determined by TOF estimation based on the assumed dielectric constant. Note that while our previous work [19] has introduced a homogeneous assumption-based CSI described above, the study in [19] assumes that the thickness is given as a prior knowledge,

Manuscript received April 30, 2021; revised June 20, 2021; accepted July 20, 2021. Date of publication August 25, 2021; date of current version January 6, 2022. This work was supported by Japan Science Technology Agency (JST), Precursory Research for Embryonic Science and Technology (PRESTO), Japan, under Grant JPMJPR1771. (Corresponding author: Shouhei Kidera.)

Hayatomomaru Morimoto and Yoshihiro Yamauchi are with the Graduate School of Informatics and Engineering, University of Electro-Communications, Tokyo 1828585, Japan.

Shouhei Kidera is with the Graduate School of Informatics and Engineering, University of Electro-Communications, Tokyo 1828585, Japan, and also with the Japan Science Technology Agency, Precursory Research for Embryonic Science and Technology (PRESTO), Saitama 332-0012, Japan (e-mail: kidera@uec.ac.jp).

Digital Object Identifier 10.1109/LGRS.2021.3099199

1558-0571 © 2021 IEEE. Personal use is permitted, but republication/redistribution requires IEEE permission.
See <https://www.ieee.org/publications/rights/index.html> for more information.

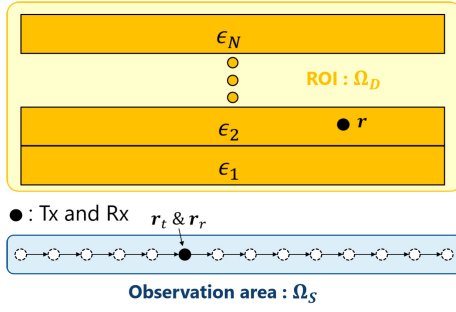


Fig. 1. Mono-static observation model and multilayered object.

which is not given in this study. A numerical test using a 2-D-FDTD forward solver indicated that the proposed method enables the estimation of both the thickness and the dielectric constant in each layer at a lower computational cost.

II. METHOD

A. Observation Model

Fig. 1 shows the observation geometry used here. It includes a set of transmitters and receivers, in which a multiple layered object with a planar structure is located in front of an array. A set of transmitters and receivers at the same position was scanned along x , i.e., a mono-static observation was assumed, the area of which is defined as Ω_S . $E^T(\omega; \mathbf{r}_t, \mathbf{r}_r)$ is the total electric field in case of a transmitting source located at \mathbf{r}_t that induces the electromagnetic wave penetrating the objects. The background medium was assumed to be air, and each layer of the object was assumed to have a homogeneous complex permittivity profile. The scattered response of the electromagnetic wave is recorded by a receiver located at \mathbf{r}_r of the angular frequency ω as: $E^S(\omega; \mathbf{r}_t, \mathbf{r}_r) \equiv E^T(\omega; \mathbf{r}_t, \mathbf{r}_r) - E^I(\omega; \mathbf{r}_t, \mathbf{r}_r)$, where $E^I(\omega; \mathbf{r}_t, \mathbf{r}_r)$ is the incident electric fields, which is observed in the case with no object. d_i and ϵ_i are the thickness and complex permittivity of the i th layer of object, respectively, which are not given.

B. Thickness Estimation: CS

The thickness estimation method is based on the CS algorithm. The CS-based TOF estimation demonstrated a considerably higher resolution than the TOF theoretical resolution [9]. In a typical THz imaging model, assuming a multilayer object, an original TOF profile has a sparse distribution in the time domain, and a sparse regularization scheme is effective in most cases. Here, the reflection response denoted $y(t; \mathbf{r}_t, \mathbf{r}_r)$ is the inverse Fourier transform of $E^S(\omega; \mathbf{r}_t, \mathbf{r}_r)$ and is given by the convolutional model as

$$y(t; \mathbf{r}_t, \mathbf{r}_r) = \sum_{i=1}^N A_i s_{\text{ref}}(t) * \delta(t - \tau_i) + n(t) \quad (1)$$

where $s_{\text{ref}}(t)$ is a reference signal (mostly a transmitted signal) and N is the number of layers. Notably, multiple reflections

$$A \equiv \begin{pmatrix} s_{\text{ref}}(K), & s_{\text{ref}}(K-1), & \dots, & s_{\text{ref}}(0), & 0, & 0, & \dots, & 0 \\ 0, & s_{\text{ref}}(K), & \dots, & s_{\text{ref}}(1), & s_{\text{ref}}(0), & 0, & \dots, & 0 \\ & & & \ddots & & & & \\ 0, & 0, & \dots, & 0, & s_{\text{ref}}(K), & s_{\text{ref}}(K-1), & \dots, & s_{\text{ref}}(0) \end{pmatrix} \quad (3)$$

between the layers are not considered in this model. The strength of such reflections will be negligible compared with that of direct reflections in the case of low dielectric contrast and lossy media. A_i and τ_i are the amplitude and time delay of the i th layer reflection, respectively. Thus, the discrete model of 1 can be represented as

$$\mathbf{y} = \mathbf{A}\mathbf{x} + \mathbf{n} \quad (2)$$

where \mathbf{y} and \mathbf{x} are the discrete forms of $y(t)$ and $x(t)$, respectively. \mathbf{n} denotes an additive white noise. $x(t)$ is the original TOF profile that can be converted into the thickness of each layer based on its relative permittivity. \mathbf{A} is called an observation matrix, which is determined by a time-shifted profile of a reference signals as shown in (3) in the bottom of the page, where K is the number of data length of the reference signal $s_{\text{ref}}(t)$. The original profile \mathbf{x} was assumed to have a sparse distribution similar to that of (1), and hence, the optimal TOF profile $\hat{\mathbf{x}}$ is given by the l_1 norm-regularized optimization

$$\hat{\mathbf{x}} = \arg \min_{\mathbf{x}} (\|\mathbf{y} - \mathbf{A}\mathbf{x}\|_2^2 + \lambda \|\mathbf{x}\|_1) \quad (4)$$

where λ is a regularization coefficient and $\|\cdot\|_m$ is the l_m norm. If the number of layers is given, we could extract the TOF value of τ_i , corresponding to the i th layer.

C. Permittivity Estimation: CSI

This study introduces the CSI-based permittivity estimation for each layer. In this section, the methodology of CSI is briefly described. Let Ω_D be the ROI, including the objects. The scattered field $E^S(\omega; \mathbf{r}_t, \mathbf{r}_r)$ is formed by the following Helmholtz-type domain integral equation (DIE):

$$E^S(\omega; \mathbf{r}_t, \mathbf{r}_r) = (k^B)^2 \int_D G^B(\omega; \mathbf{r}_r, \mathbf{r}) w(\omega; \mathbf{r}_t, \mathbf{r}) d\mathbf{r} \quad (5)$$

where k^B is the wavenumber of the background medium and $G^B(\omega; \mathbf{r}_r, \mathbf{r})$ is Green's function of the background medium. $w(\omega; \mathbf{r}_t, \mathbf{r}) \equiv E^T(\omega; \mathbf{r}_t, \mathbf{r}_r) \chi(\omega; \mathbf{r})$ is called the contrast source defined by $\chi(\omega; \mathbf{r}) \equiv \epsilon(\omega; \mathbf{r}) / \epsilon^B(\omega; \mathbf{r}) - 1$, where $\epsilon(\omega; \mathbf{r})$ and $\epsilon^B(\omega; \mathbf{r})$ are the complex permittivity with and without an object at the angular frequency ω , respectively. The CSI focuses on the principle that (5) should be satisfied for the regions corresponding not only to $\mathbf{r} \in \Omega_S$ (the data equation) but also to $\mathbf{r} \in \Omega_D$ (the state equation).

Thus, instead of numerically calculating $E^T(\omega; \mathbf{r}_t, \mathbf{r}_r)$ in the ROI, the CSI simultaneously optimizes the object function χ and E^T via the contrast source variable w as follows:

$$F(\chi, w) \equiv \frac{\sum_{\mathbf{r}_t} \|E^S(\omega; \mathbf{r}_t, \mathbf{r}_r) - \mathcal{G}^S[w]\|_{\Omega_S}^2}{\sum_j \|E^S(\omega; \mathbf{r}_t, \mathbf{r}_r)\|_{\Omega_S}^2} + \frac{\sum_{\mathbf{r}_t} \|\chi(\mathbf{r}) E^I(\omega; \mathbf{r}_t, \mathbf{r}') - w(\omega; \mathbf{r}_t, \mathbf{r}) + \chi(\mathbf{r}) \mathcal{G}^D[w]\|_{\Omega_D}^2}{\sum_{\mathbf{r}_t} \|\chi(\omega; \mathbf{r}) E^I(\omega; \mathbf{r}_t, \mathbf{r}')\|_{\Omega_D}^2} \quad (6)$$

Here, the following notations are defined as

$$\mathcal{G}^S[w] = (k^B)^2 \int_{\Omega_D} G^B(\omega; \mathbf{r}_r, \mathbf{r}) w(\omega; \mathbf{r}_t, \mathbf{r}) d\mathbf{r}, \quad (\mathbf{r} \in \Omega_D) \quad (7)$$

$$\mathcal{G}^D[w] = (k^B)^2 \int_{\Omega_D} G^B(\omega; \mathbf{r}', \mathbf{r}) w(\omega; \mathbf{r}_t, \mathbf{r}) d\mathbf{r}, \quad (\mathbf{r}' \in \Omega_D) \quad (8)$$

where $\|\cdot\|_{\Omega_S}^2$ and $\|\cdot\|_{\Omega_D}^2$ are l_2 norms defined in the area of Ω_S and Ω_D , respectively. The three variables, $w(\mathbf{r}_t, \mathbf{r})$, $E^T(\omega; \mathbf{r}_t, \mathbf{r}_r)$, and $\chi(\omega; \mathbf{r})$ are sequentially updated to minimize the cost function in (6) [15]. Namely, the total field $E^T(\omega; \mathbf{r}_t, \mathbf{r}_r)$ is automatically determined, and hence, there is no need for an iterative use of computationally expensive forward solver, such as FDTD.

D. Proposed Method

The CSI method provides a quantitative estimate of complex permittivity. However, it is inaccurate when the number of unknowns is larger than that of data samples, which would have occurred in the scenario assumed in this study, Fig. 1. This study then introduces a reduction scheme of the number of unknowns, assuming that each layer has a homogeneous medium with the same complex permittivity, which is defined as the unknown set: $\chi \equiv (\chi_1, \dots, \chi_n, \dots, \chi_N)$, where χ_n is the contrast function of the n th layer. Thus, the estimation problem for the permittivity of each layer is given by

$$\hat{\chi} = \arg \min_{\chi} \sum_{n=1}^N F(\chi_n, w_n; \Omega_{D,i}) \quad (9)$$

w_n is the contrast source, which is optimized in the CSI scheme using an initial set of χ . $F(\chi_n, w_n; \Omega_{D,i})$ is the cost function, when the integral area of Ω_D is updated to be $\Omega_{D,i}$. Note that (6) includes the interactions between multiple layers, because a cost function $F(\chi_n, w_n; \Omega_{D,i})$ defined in each layer is calculated by considering the interactions with other layers, that is, the contrast source $w(\mathbf{r}_t, \mathbf{r})$ in each layer must be affected by those in the other layers. Here, the ROI for the i th layer, which is denoted as $\Omega_{D,i}$, is determined by each thickness of the i th layer, which is calculated as

$$\hat{d}_i = c_{\text{air}} \tau_i / \sqrt{\Re[\epsilon_i]} \quad (10)$$

where c_{air} is the propagation speed in air, and τ_i is the TOF determined by the CS filtering process given in (4). Note that only the variable w_n is updated in each CSI process with a fixed χ_n to calculate a residual of the cost function $F(\chi_n, w_n)$, assuming an initial set of χ .

The actual procedure of the proposed method is summarized as follows:

Step 1: Reflection response denoted $y(t; \mathbf{r}_t, \mathbf{r}_r)$ is processed using the CS filter as shown in (4) and a TOF response τ_i is obtained for each layer based on the local peaks of the reconstruction response of $\hat{\chi}$.

Step 2: Using a variable set in a contrast function as $\chi \equiv (\chi_1, \dots, \chi_n, \dots, \chi_N)$, the ROI domain $\Omega_{D,i}$ is calculated using the thickness of each layer \hat{d}_i obtained from (10).

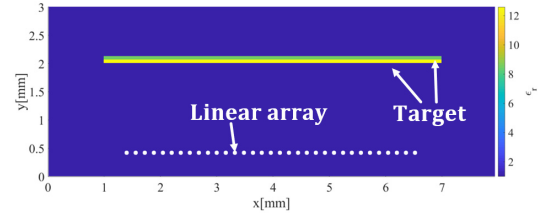


Fig. 2. Simulation model. Color denotes a real part of complex permittivity. White solid circles are sampling points of the observation.

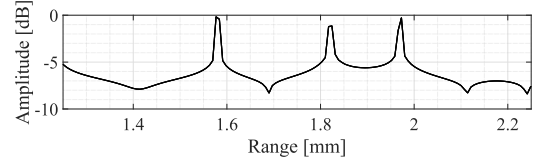


Fig. 3. Example of the CS filter response. The horizontal axis denotes the optical distance.

Step 3: Cost function given in (9) is calculated using χ and $\Omega_{D,i}$.

Step 4: χ is updated until the convergence criteria are satisfied.

The thickness of each layer \hat{d}_i is not updated in the CSI iteration sequence but is used by a prior estimation of the ROI with the given relative permittivity ϵ_i . If the assumed permittivity set in χ is different from the original profile, the thickness of each layer, that is, its ROI, would also be far from the actual one, which causes an insufficient convergence of the cost function in CSI. Thus, this method could simultaneously estimate both the thickness and permittivity of each layer, by exploiting the features of the CSI process.

III. NUMERICAL TEST

A. Numerical Setting

A 2-D FDTD-based numerical simulation was conducted for each method. Fig. 2 shows the numerical model assumed in this section. A cell size of $20 \mu\text{m}$ was set for FDTD and CSI. A set of a transmitter and receiver was scanned along the x -axis using equal spacing as 0.16 mm at $y = 0$, namely, 33 samples were scanned. Two-layered homogeneous objects are surrounded by air. The width (along the x -axis) and thickness (along the y -axis) of the object are 6.0 and 0.06 mm , respectively. Each complex permittivity was set to $(\Re[\epsilon_1], \Re[\epsilon_2]) = (12.58 + 1.31j, 8.42 + 0.57j)$ for the first and second layers, respectively, at 0.20 THz . Namely, the theoretical range resolutions in air is 0.75 mm . A TM-mode wave was assumed, and a Gaussian modulated pulse (center frequency = 0.24 THz and bandwidth = 0.27 THz) was used as the source current waveform. The CSI was conducted using a maximum iteration number of 20000, using only single-frequency data of 0.20 THz . If the inversion cell size, including the objects of the two layers, was set to $20 \mu\text{m}$, the number of unknowns becomes 1800 (6×300), while that of the data samples is 33, i.e., a much ill-conditioned model was assumed. For simplicity, the conductivity of each layer was given in all methods.

B. TOF Estimation Results

At first, the TOF estimation by CS filtering in (4) is investigated. Fig. 3 shows the CS responses, namely, $\hat{\chi}$ in (4),

TABLE I
TOF ESTIMATION RESULTS BY THE CS FILTER

	Original	Estimation
1st TOF (1st layer's front surface)	1.60 mm	1.58 mm
2nd TOF (1st layer's backside surface)	1.81 mm	1.82 mm
3rd TOF (2nd layer's backside surface)	1.98 mm	1.97 mm

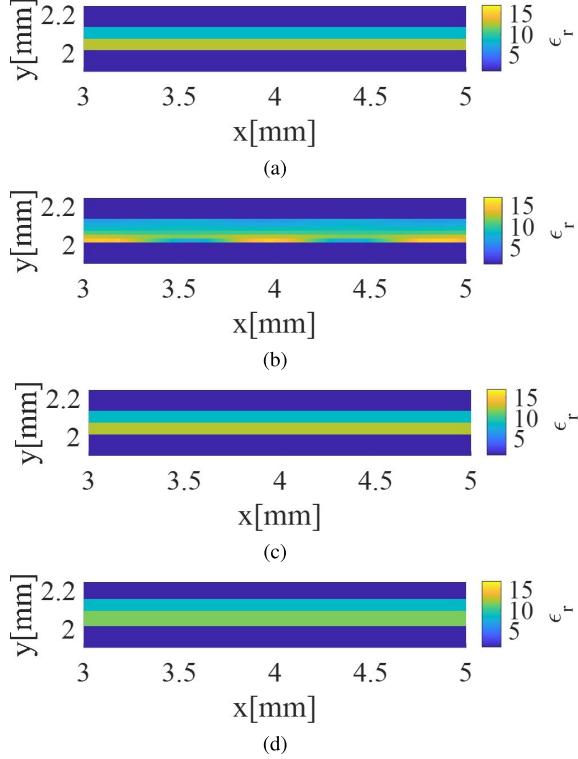


Fig. 4. Reconstruction results by each method. Color scale denotes the real part of complex permittivity. (a) True profile. (b) Original CSI. (c) Proposed CSI (thickness: given). (d) Proposed CSI (thickness: not given).

where λ is empirically adjusted to 2.0×10^{-5} . As indicated in the figure, three distinguished peaks were observed within a 2-mm range. The first, second, and third peaks correspond to the surface reflections from the first layer, the interface between the first and second layers, and the backside of the second layer, respectively. Multiple reflections were received at a later time, which could not be recognized in this figure. The thickness of each layer, i.e., ROI, in the CSI scheme, which depends on the permittivity value selected from χ , can be determined based on these three TOF values. Table I presents a comparison between the original and estimated TOF profiles for this case. It demonstrated that the CS filter provides a considerably accurate and super-resolution TOF estimation even in a very thin-layer model (the theoretical optical range resolution is 0.75 mm), in which the error is within a cell size (0.02 mm) of the FDTD or CSI calculation. Notably, we confirmed that if the TOF is exactly on the discretization cell, its CS response perfectly reconstructs the true TOF profile, indicating that this problem almost satisfies the perfect recovery condition. In this case, although the true TOFs are not exactly on the discretization cell, the reconstruction results are slightly spread into the neighboring cell, as shown in Fig. 3.

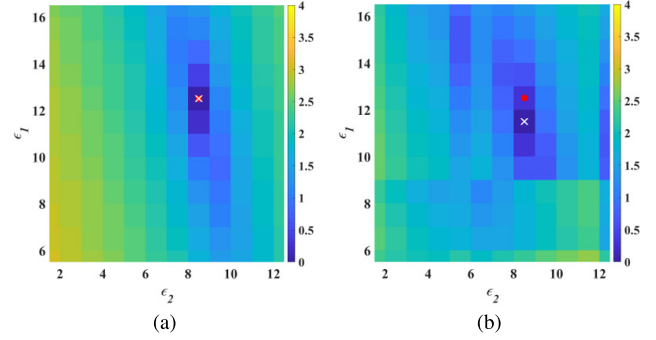


Fig. 5. Residual of cost function in the CSI for each combination of (ϵ_1, ϵ_2) . Red solid circles and white X denote the original and optimized combination of (ϵ_1, ϵ_2) , respectively. Color denotes the cost function of the CSI as $F(\chi, w)$ in log scale. (a) Proposed CSI (thickness: given). (b) Proposed CSI (thickness: not given).

C. Permittivity and Thickness Estimation Results

Next, permittivity and thickness analyses were conducted. Fig. 4(b) shows the reconstruction results obtained by the original CSI, in which an initial estimate is given by the background medium (vacuum). These results show that the permittivity reconstruction by the original CSI is significantly inaccurate due to the ill-conditioned model that has a considerably large number of unknowns (1800). In the method proposed here, the search ranges of relative permittivity of the first and second layers were $5.5 \leq \epsilon_1 \leq 16.5$ and $1.5 \leq \epsilon_2 \leq 12.5$, respectively. A full search (with the sampling interval for $\Re[\epsilon_1]$ and $\Re[\epsilon_2]$, $\Delta\epsilon = 1$) was applied. Thus, 144 combinations were assessed to determine the set of $(\Re[\epsilon_1], \Re[\epsilon_2])$. The ROI of each layer $\Omega_{D,i}$ in (9) is determined using $\Re[\epsilon_i]$ and \hat{d}_i . Fig. 5 shows the residual of the cost function determined in (9) when the thickness of each layer was given or not given. As shown in Fig. 5(a), when the thickness was known, there was only one local minimum, which is also a global minimum, close to the actual permittivity combination $(\Re[\epsilon_1], \Re[\epsilon_2]) = (12.5, 8.5)$. When the thickness was not given but estimated by the CS-based TOA estimator, there was a minimum point close to the actual one $(\Re[\epsilon_1], \Re[\epsilon_2])$, which demonstrates that the proposed method could simultaneously estimate both the thickness and permittivity with high accuracy. Fig. 4(c) and (d) shows the results obtained by the proposed method when the thickness was given or not given and verified that the proposed method offers accurate dielectric profile even in a considerably ill-posed situation. Table II shows the root mean square errors (RMSEs) of the reconstruction results, necessary computational costs, and thickness estimation obtained by each method, using an Intel(R) Xeon(R) Gold 6130 central processing unit (CPU), a 2.10-GHz processor, and a 704-GB random access memory (RAM). Quantitative error analysis was conducted based on the RMSE of the real complex permittivity

$$\text{RMSE}_{\Re[\epsilon]} = \sqrt{\frac{1}{K} \sum_{k=1}^K |\Re[\epsilon^{\text{true}}(\mathbf{r}_k)] - \Re[\hat{\epsilon}(\mathbf{r}_k)]|^2} \quad (11)$$

where $\Re[\epsilon^{\text{true}}(\mathbf{r}_k)]$ and $\Re[\hat{\epsilon}(\mathbf{r}_k)]$ are the real parts of the complex permittivity of the true and estimated values, respectively. K is the total number of cells in ROI. The results

TABLE II
COMPARISON OF RMSES, CALCULATION TIMES, AND THICKNESS OBTAINED BY EACH METHOD

Method	Estimations of (ϵ_1, ϵ_2)	RMSEs of $\Re[\epsilon]$	Computational time	Estimated Thickness (d_1, d_2)
Original CSI	N/A	1.91	5.54×10^3 s	(0.6mm, 0.6mm)
Proposed CSI (Thickness: Given)	(12.5, 8.5)	0.08	1.98×10^3 s	N/A
Proposed CSI (Thickness: Not Given)	(11.5, 8.5)	0.77	7.69×10^3 s	(0.6mm, 0.6mm)

in Table II prove that while the proposed method requires a slightly larger computational cost, the reconstruction accuracy is considerably improved, compared with that of the original CSI. Furthermore, as shown in Table II, the proposed method offers an accurate thickness estimation in each layer. These results demonstrated that the proposed method gives an accurate relative permittivity profile, without a prior knowledge of the thickness of each layer. Although (10) does not consider the imaginary parts of the complex permittivity, the relative difference between the cases considering and not considering the imaginary parts is 0.43% for d_1 and 0.057% for d_2 . These differences are almost negligible. Furthermore, this study assumes that the actual conductivity of each layer is given in the estimation. However, we demonstrated that these conductivities do not affect the estimation performance of the relative permittivity and thickness. It is considered that the CSI's cost function is much more sensitive to an error in $\Re[\epsilon]$, than to that in $\Im[\epsilon]$, because the TOF estimation errors (affected by $\Re[\epsilon]$) will be dominant over the signal strength variation (affected by $\Im[\epsilon]$) in this case.

IV. CONCLUSION

This study introduced a hybrid algorithm using a CS filter-based thickness estimation and CSI-based relative permittivity reconstruction for multilayered objects using THz-band analysis. This method offers an accurate estimation for both the thickness and relative permittivity of multilayered objects, which was not previously achieved by any other approach. In addition, combination searches for relative permittivities were conducted to avoid a local minimum problem, and each thickness, i.e., the ROI of objects, was simultaneously determined using a minimization problem of the CSI cost function. CSI requires a significant computational time compared with other TOF-based estimation approaches. However, it could determine the dielectric profile, including a multiple scattering phenomenon among the layers, of which the component was considered in the DIE of (5). This numerical test to assess the systematic error in each method has no noise. However, the effectiveness of the CS filter or CSI in a noisy scenario was demonstrated in [9] and [9] or [15]. The experimental validation of this method is included in our future scope. Notably, thickness estimation based on (10) assumes the monostatic observation model, in which the incident angle should be zero; this model should be extended to include arbitrary incident angles to deal with a multistatic observation model.

REFERENCES

- [1] K. Kawase, Y. Ogawa, Y. Watanabe, and H. Inoue, "Non-destructive terahertz imaging of illicit drugs using spectral fingerprints," *Opt. Exp.*, vol. 11, no. 20, p. 2549, Oct. 2003.
- [2] R. Fukusawa, "Terahertz imaging: Widespread industrial application in non-destructive inspection and chemical analysis," *IEEE Trans. Terahertz Sci. Technol.*, vol. 5, no. 6, pp. 1121–1127, Nov. 2015.
- [3] Y. Jiang, H. Wang, Y. Qin, B. Deng, J. Gao, and Z. Zhuang, "A three-dimensional surface imaging method using THz dual-frequency interferometry," *IEEE Geosci. Remote Sens. Lett.*, vol. 13, no. 11, pp. 1651–1655, Nov. 2016.
- [4] T. Matsui and S. Kidera, "Virtual source extended range points migration method for auto-focusing 3-D terahertz imaging," *IEEE Geosci. Remote Sens. Lett.*, vol. 18, no. 6, pp. 989–993, Jun. 2021.
- [5] H. Liu *et al.*, "Dimensionality reduction for identification of hepatic tumor samples based on terahertz time-domain spectroscopy," *IEEE Trans. Terahertz Sci. Technol.*, vol. 8, no. 3, pp. 271–277, May 2018.
- [6] D. M. Hailu, A. K. Ayesheshim, and D. Saeedkia, "Multi-layer plastic bottle and preform thickness measurement using terahertz pulses," in *Proc. Photon. North (PN)*, May 2016, pp. 1–4.
- [7] D. M. Mittleman, S. Hunsche, L. Boivin, and M. C. Nuss, "T-ray tomography," *Opt. Lett.*, vol. 22, no. 12, pp. 904–906, 1997.
- [8] S. Krimi, J. Jonuscheit, G. Von Freymann, R. Urbansky, and R. Beigang, "Highly accurate thickness measurement of multi-layered automotive paints using terahertz technology," *IEEE Trans. Geosci. Remote Sens.*, vol. 48, no. 4, pp. 1993–2004, Apr. 2010.
- [9] H. Morimoto and S. Kidera, "Super-resolution multilayer structure analysis via depth adaptive compressed sensing for terahertz subsurface imaging," *IEEE Geosci. Remote Sens. Lett.*, early access, Dec. 21, 2020, doi: [10.1109/LGRS.2020.3043481](https://doi.org/10.1109/LGRS.2020.3043481).
- [10] K. M. Golden *et al.*, "Inverse electromagnetic scattering models for sea ice," *IEEE Trans. Geosci. Remote Sens.*, vol. 36, no. 5, pp. 1675–1704, Sep. 1998.
- [11] M. Nakhkash, Y. Huang, and M. T. C. Fang, "Application of the multilevel single-linkage method to one-dimensional electromagnetic inverse scattering problem," *IEEE Trans. Antennas Propag.*, vol. 47, no. 11, pp. 1658–1668, Nov. 1999.
- [12] T. Uno and S. Adachi, "Inverse scattering method for one-dimensional inhomogeneous layered media," *IEEE Trans. Antennas Propag.*, vol. 35, no. 12, pp. 1456–1466, Dec. 1987.
- [13] W. C. Chew and Y. M. Wang, "Reconstruction of two-dimensional permittivity distribution using the distorted Born iterative method," *IEEE Trans. Med. Imag.*, vol. 9, no. 2, pp. 218–225, Jun. 1990.
- [14] M. D'Urso, T. Isernia, and A. F. Morabito, "On the solution of 2-D inverse scattering problems via source-type integral equations," *IEEE Trans. Geosci. Remote Sens.*, vol. 48, no. 3, pp. 1186–1198, Mar. 2010.
- [15] P. M. van den Berg and A. Abubakar, "Contrast source inversion method: State of art," *Prog. Electromagn. Res.*, vol. 34, pp. 189–218, 2001.
- [16] P. M. van den Berg, A. L. V. Broekhoven, and A. Abubakar, "Extended contrast source inversion," *Inverse Problems*, vol. 15, no. 5, pp. 1325–1344, 1999.
- [17] D. L. Donoho, "Compressed sensing," *IEEE Trans. Inf. Theory*, vol. 52, no. 4, pp. 1289–1306, Apr. 2006.
- [18] J. L. Dong, X. L. Wu, A. Locquet, and D. S. Citrin, "Terahertz super-resolution stratigraphic characterization of multilayered structures using sparse deconvolution," *IEEE Trans. Terahertz Sci. Technol.*, vol. 7, no. 3, pp. 260–267, May 2017.
- [19] H. Morimoto and S. Kidera, "Complex permittivity reconstruction for multi-layered object by low complexity contrast source inversion method," in *Proc. 45th Int. Conf. Infr., Millim., Terahertz Waves (IRMMW-THz)*, Nov. 2020, pp. 1–2.